# Beta Mixture Model for the Uncertainties in Robotic Haptic Object Identification

Yu Xia, *Graduate Student Member, IEEE*, Alireza Mohammadi, Liuhua Peng, Ying Tan, *Senior Member, IEEE*, Bernard Chen, Peter Choong, and Denny Oetomo, *Senior Member, IEEE*

***Abstract*—Robotic haptic object identification is the process to identify objects out of a given object set using a robotic hand equipped with tactile and finger-joint displacement sensors. When taking measurements by grasping the object, the uncertainties in the pose of the object relative to the hand will adversely affect the identification accuracy. Each tactile sensor measures contact in its locality, thus, a change in object contact locations relative to the robotic grasping hand significantly affects the tactile measurements. In object identification, statistical properties of the uncertainties in the collected measurements are generally obtained *a priori*, allowing the probabilities of an object to be estimated for improved accuracy. The problem of object pose uncertainty typical in robotic grasping results in multiple peaks in the probability distribution of the resulting tactile measurements. The peaks are associated with whether or not the (locality of) tactile sensor on the robotic hand is in contact with the object due to the variations in object pose. As such, in this article, a Beta mixture model allowing multiple peaks in the distribution is proposed to represent this object pose uncertainty (relative to the robotic hand) in place of the conventional Gaussian model used in the literature. The method was experimentally validated and demonstrated to be effective in capturing the uncertainties and improving the accuracy of the haptic object identification.**

***Index Terms*—Beta mixture model, haptic object identification, robotic grasping, tactile sensing.**

Manuscript received 18 January 2022; revised 25 March 2022; accepted 23 April 2022. Date of publication 2 June 2022; date of current version 16 August 2022. Recommended by Technical Editor Z. Chen and Senior Editor X. Chen. This work was supported by the Valma Angliss Trust. *(Corresponding author: Denny Oetomo.)*

Yu Xia, Alireza Mohammadi, Ying Tan, Bernard Chen, and Denny Oetomo are with the Department of Mechanical Engineering, The University of Melbourne, Melbourne, VIC 3010, Australia (e-mail: yxia3@student.unimelb.edu.au; alireza.mohammadi@unimelb.edu.au; yingt@unimelb.edu.au; bernard.chen@unimelb.edu.au; doetomo@unimelb.edu.au).

Liuhua Peng is with the School of Mathematics and Statistics, The University of Melbourne, Melbourne, VIC 3010, Australia (e-mail: liuhua.peng@unimelb.edu.au).

Peter Choong is with the Department of Surgery, St Vincent's Hospital, The University of Melbourne, Melbourne, VIC 3010, Australia (e-mail: pchoong@unimelb.edu.au).

Color versions of one or more figures in this article are available at https://doi.org/10.1109/TMECH.2022.3175491.

Digital Object Identifier 10.1109/TMECH.2022.3175491

## I. Introduction

HAPTICS is an important sensing modality for perceiving the physical and surface properties of objects and the interaction forces between the end-effectors and the objects [1], [2]. Haptic object identification, which is often used in object manipulation learning [3], [4], industrial assembly [5], [6], and underwater applications [7], is one of the applications of haptics. It plays an important role when the identification process needs to rely on the information provided only through the physical interaction between the end-effector and the objects, or when the process cannot be conveniently achieved by other means [8]. While haptics is most likely used in conjunction with other sensing modalities in practice (e.g., with vision) [9], [10], it is also important for haptic object identification to be studied in isolation to understand the extent of its capabilities. This article focuses on performing object identification using a robotic hand equipped with tactile and finger-joint displacement sensors without other sensing modalities. Such a setting can also be found in [11] and [12].

Since haptic information can only be obtained by contacting the objects, it is essential to consider the exploratory procedure of haptic identification [14]. In the literature on robotic haptic identification, different procedures are adopted. Specifically, [12] and[15]–[19] did the enclosure (such as grasping or touching) with the objects, [20]–[23] performed the lateral motion on the surface of the objects to obtain the surface information, [11] and [24] pressed the object to identify the stiffness, [25] and [26] collect the haptic information using the static contact and unsupported holding respectively.

Among the exploratory procedures, the enclosure is one of the most commonly used procedures as it is informative and relatively fast to be executed [27]. However, the information collected by grasping/touching objects has the problem that for the fixed locations of tactile sensors on the robotic hand, the measurements are dependent upon the contact pose of the object relative to the hand at grasping, such as shown in Fig. 1. In other words, the measurements of each sensor (embedded on specific locations the robotic hand/grasper used to perform the grasping and touching) will be susceptible to the error in the relative pose between the object and the grasper. Given the high likelihood of the uncertainties in this relative pose, it introduces a significant source of uncertainties in the problem.

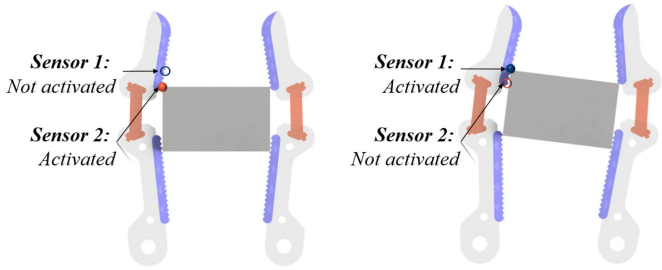


Fig. 1. Illustrative example showing the impact of uncertain contact positions in the measurements (The finger model is referenced from [13]). (a) In the first grasp, Sensor 1 is not activated while Sensor 2 is activated. (b) In the second grasp, Sensor 1 is activated while Sensor 2 is not activated.

To address the challenges introduced by the above mentioned uncertainties, three methodologies have been proposed in the literature on haptic identification. The first is machine learning-based methods (such as neural networks) [15], [17], [28]–[30], though the performance of machine learning techniques relies on the selected structure and parameters, which usually are selected by trial-and-error. Using inappropriate parameters or structures might lead to a poor identification performance as indicated in [31] and [32]. Moreover, as a typical black-box identification technique, the results are lack of interpretability, which might limit the scope of the methods in some applications, such as medical, in which interpretability plays an important role in diagnosis as pointed out in [33].

The second method extracts features, which are less sensitive to uncertainties, in haptic object identification, see, for example, [12], [18], [26], [34]–[36], and references therein. However, with different end-effectors and different types or numbers of embedded sensors, the features that can be extracted are different. Therefore, finding features, which keep the majority of information from sensors and are less sensitive to uncertainties, might be challenging sometimes [32].

The third is to use statistical modeling techniques to perform haptic object identification from measured data [20], [25]. Given a set of collected haptic measurements, the statistical model can characterize the distribution of measurements offline. This information can be utilized to understand the patterns within this dataset. Consequently, this statistical model is used to interpret the likelihood that a testing measurement belongs to an object, based on the prior knowledge of the dataset [37]. Compared to machine learning-based techniques, the statistical approach provides interpretable results from physical measurements. Compared to feature extraction techniques, this technique utilizes all information measured from sensors and further reduces the subjective human involvement in the selection of appropriate features, making it more systematic.

One of the challenges of the statistical approach is to select the model of measurements. The Gaussian model has been used to account for the tactile sensor noise [20], [25]. However, it is questionable that a Gaussian model is able to cope with uncertainties. When a robotic hand is grasping an object, the probability density function ($pdf$) of tactile sensor measurements generally has more than one peak. As shown in Fig. 1, for objects other than perfect cylinders or spheres in shape, when grasped at different postures, tactile sensors on a given location of the robotic hand may or may not come into contact with the object. With a slight amount of uncertainties between the hand and the object, the resulting $pdf$ of the measurement of a tactile sensor will peak around the "no contact" case and the "firm contact" case. The Gaussian model, which is typically used in many existing algorithms, is not a good candidate to characterize the $pdf$ of tactile sensors as it is symmetrically distributed and only works when most data are around the central peak.

The Beta model is a family of continuous probability distributions defined for a normalized random variable parameterized by two positive shape parameters. The Beta mixture model (BMM) is an extension of the Beta model. It combines multiple Beta models to accommodate $pdf$ with multiple peaks, presenting the advantage of characterising the uncertainties in the haptic measurements.

In order to test the effectiveness and practicability of the BMM, the Reflex TakkTile robotic hand with integrated joint displacement and tactile sensors is used to perform the object identification from the set consisting of 20 objects. In particular, to provide insight of choosing the parameters of the proposed algorithm, the experiments analyze the balance between model complexity [the number of BMMs (or segments) used to describe the haptic information of an object], the number of repetitions of each grasp, and identification accuracy.

By investigating the nature of uncertainty distribution in haptic information typical in object grasping for object identification, it was found that the distribution is not typical Gaussian but has multiple peaks associated with whether the locality of the tactile sensors onboard the robotic hand is in contact with the object due to the variation in object pose. Incorporating a BMM to account for this uncertainty distribution was shown experimentally to increase the accuracy of object identification.

## II. Preliminaries

This section provides preliminaries, including the introduction of the Beta mixture model, problem formulation, and the procedure of haptic object identification.

### A. Beta Mixture Model

*1) Beta Model:* For $x \in [0, 1]$, the probability density function ($pdf$) of a Beta model [38] is defined as

$$f^{\boldsymbol{\theta}}_{\text{beta}}(x) = \frac{x^{\alpha-1}(1-x)^{\beta-1}}{\mathbf{B}(\alpha,\beta)} = \frac{x^{\alpha-1}(1-x)^{\beta-1}}{\int_0^1 u^{\alpha-1}(1-u)^{\beta-1}du} \quad (1)$$

where $\alpha$ and $\beta$ are positive shape parameters of $pdf$. $\mathbf{B}(\alpha,\beta)$ is the function that ensures the total probability is one. Here, $\boldsymbol{\theta} = [\alpha, \beta]$ represents the parameter vector.

*2) Beta Mixture Model:* The BMM is a combination of $K$ Beta models, where $K \in \mathcal{N}_{>0}$ is called the number of components of the BMM. Here, $\mathcal{N}_{>0}$ is the set of positive integers. The

$pdf$ of the BMM can be represented as

$$f_{mix}^{\boldsymbol{\theta}_{mix}}(x) = \sum_{k=1}^{K} \pi_k f_{\text{beta}}^{\boldsymbol{\theta}_k}(x) = \sum_{k=1}^{K} \pi_k \left[ \frac{x^{\alpha_k - 1}(1-x)^{\beta_k - 1}}{\int_0^1 u^{\alpha_k - 1}(1-u)^{\beta_k - 1} du} \right] \quad (2)$$

where $\boldsymbol{\theta}_k = [\alpha_k, \beta_k]^T$ is the parameter vector of the $k^{\text{th}}$ component of $pdf$, $\pi_k$ is the mixture coefficient of the $k^{\text{th}}$ component which satisfies $\pi_k \geq 0$ and $\sum_{k=1}^{K} \pi_k = 1$. In (2), $\boldsymbol{\theta}_{mix} = \left[\pi_1, \boldsymbol{\theta}_1^T, \pi_2, \boldsymbol{\theta}_2^T, \ldots, \pi_K, \boldsymbol{\theta}_K^T\right]^T \in LP^{3K}$ is the lumped parameter vector, where $LP^{3K} = \left\{ \left[\pi_1, \boldsymbol{\theta}_1^T, \pi_2, \boldsymbol{\theta}_2^T, \ldots, \pi_K, \boldsymbol{\theta}_K^T\right]^T : \sum_{k=1}^{K} \pi_k = 1, \pi_k \geq 0, \alpha_k > 0, \beta_k > 0 \text{for} k = 1, \ldots, K \right\}$ is the parameter space.

*3) Maximum Likelihood Estimation (MLE):* For a set of measurements $(x_1, \ldots, x_c, \ldots, x_N)$ (or the dataset $D$), it is assumed that the measurements satisfy the BMM with the unknown $\boldsymbol{\theta}_{mix}$. The maximum likelihood estimation (MLE) method [39] has the following cost function:

$$\underset{\boldsymbol{\theta}_{mix} \in LP^{3K}}{\text{maximize}} \ \mathcal{L}(\boldsymbol{\theta}_{mix}) \quad (3)$$

where $\mathcal{L}(\boldsymbol{\theta}_{mix}) = \sum_{c=1}^{N} \ln f_{mix}^{\boldsymbol{\theta}_{mix}}(x_c)$. It is noted that the higher dimension of $\boldsymbol{\theta}_{mix}$, the more data are needed to accurately estimate the parameters using the MLE. If the dataset is not rich enough, there will be a nonnegligible bias in the parameter estimation.

### B. Problem Formulation of Haptic Object Identification

For a given set of objects $O$, defined as $O = \{o_1, \ldots, o_\ell\}$, $\ell \in \mathcal{N}$, the aim of haptic object identification is to identify an object presented to the algorithm, among possible objects in the object set.

It should be highlighted that this article works on haptic identification (identify the specific object from a given object set) rather than haptic classification. This is currently the case as haptic is relatively less advanced than computer vision research and the information content in haptic is more sparse.

### C. Procedure of Haptic Object Identification

The procedure involved in haptic object identification includes the object dataset construction and object identification.

*1) Object Dataset Construction:* To construct the dataset, each object $o_i \in O$ (where $i \leq \ell, i \in \mathcal{N}$) will be grasped in different poses multiple times depending on the tasks, and the corresponding haptic measurements of each object at different poses will be recorded in the dataset. The collected measurements then will be used for further processing to represent the characteristics of each object.

*2) Object Identification:* In this step, the identification algorithm is presented with an object randomly selected from the object set $O$. By grasping the object, the haptic measurements will be acquired and subsequently be processed to compare with the haptic characteristics of each object in the constructed dataset. The identification algorithm will output the predicted label of the tested object, and a binary identification result (correctly identified or misidentified) will be obtained by comparing the predicted label of the object with its ground truth label. The performance of the haptic identification will be evaluated by running the process multiple times and taking the average of the number of times the algorithm correctly identifies an object out of the total number of attempts.

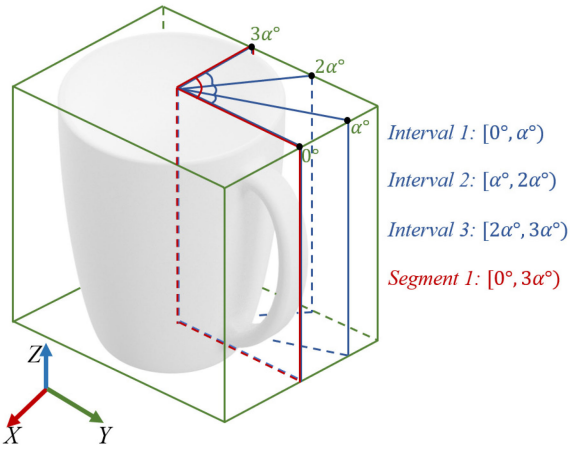


Fig. 2. Characteristics of an object are regarded to be captured by grasping the object at different intervals (only three intervals are shown). In this illustrative example, one segment contains three intervals.

Each object identification attempt can be an iterative process. During each iteration, once the haptic measurements are obtained, the identification algorithm will calculate the similarity between the object under test and each object $o_i$ in the object set $O$. When the identification procedure satisfies the stopping rule, the algorithm will stop, and the label of the object in the set $O$ with the maximum probability of similarity will output as the predicted label.

There are two stopping rules used in the literature. 1) The similarity between the object under test and one of the objects in the object set $O$ reaches a predefined threshold $\tau_b$ [25], [26]. 2) The number of grasps performed in one identification trial reaches the threshold $\tau_g$ [19], [20]. These thresholds are subjectively defined according to different needs or tasks. Both rules can be used to stop the process.

## III. Proposed Methodology

### A. Object Dataset Construction

*1) Data Acquisition and Normalization:* Each object will be split into $N_g$ uniform distributed orientation intervals along the vertical axis ($+Z$ axis), as shown in Fig. 2 (e.g., interval 1 is $[0, \alpha^o)$, referring to the first $\alpha$ degrees of the object, rotating on the $+Z$ axis). Therefore, after grasping at $N_g$ intervals, all parts of the object, at all angular displacements measured from a reference frame attached to the object, have been encapsulated by the grasp of the robotic hand. In other words, the robotic hand would collect all the haptic information necessary to describe the object. Each grasp on the object will yield an $M$ dimensional

measurement $\hat{\mathbf{z}} = [\hat{z}^1, \ldots, \hat{z}^j, \ldots, \hat{z}^M]^T$, corresponding to the number of sensors on the robotic hand. To account for the expected amount of uncertainty associated with the grasping process, in each interval, the grasp will be carried out $N_T$ times, and each time the grasp orientation relative to the object will be randomly determined.

In this article, the grasps are performed on a single height of the object for simplicity of the experimental procedure, such as practised in [11] and [35], where all objects are distinguishable from the haptic information at this height. In general, the grasp poses of objects can be extended to different heights as per the information requirement of the dataset [40].

Due to the different dimensions associated with the different types of physical variables involved (joint displacement and tactile pressure), a normalization method is needed to remove the influence of the dimension and the unit. In this article, the "Min–Max" normalization method [41], which scales the values of all variables to the range of zero and one, is employed. It is highlighted that such a normalization process is compatible with the requirement of the BMM for a normalized random variable supported on [0,1]. In summary, for $\ell$ objects in the object set, the dataset consists of $\ell \times N_g \times N_T$ total measurements. Each measurement is a $M$-dimensional vector, representing $M$ sensors used.

*2) Estimation of Parameters of Beta Mixture Model:* For each interval of the object, the measurements of each sensor should have a statistical model to capture the uncertainties for $N_T$ repetitions. Therefore, $\ell \times N_g \times M$ BMMs are required in total. In this article, we fix $N_T$ to simplify the data collection. Therefore, to have enough measurements to estimate the parameters of each BMM, the concept of the segment is introduced. A segment combines the measurements collected at a few intervals to estimate the parameters of one BMM. The number of segments is defined as $N_s = \frac{N_g}{n}$ for some $n \in \mathcal{N}$. Fig. 2 shows an example of a segment containing three intervals.

*a) Reorganizing data into segments:* The measurements in the dataset are reorganized in terms of $N_s$ segments. For each object, each segment will contain all measurements from $n$ intervals (as shown in Fig. 2), leading to $S$ measurements for the parameters estimation, where $S = N_T \times n$. For the $r^{\text{th}}$ segment $s_r$ of object $o_i$, a dataset $D_{r,i} := \{\hat{\mathbf{z}}^1_{r,i}, \ldots, \hat{\mathbf{z}}^c_{r,i}, \ldots, \hat{\mathbf{z}}^S_{r,i}\}$, where $\hat{\mathbf{z}} \in \mathcal{R}^M$, represents the readings of $M$ sensors in the collected dataset. As the subset of $D_{r,i}$, $\bar{D}^j_{r,i}$, which represents the measurements of the $j$th sensor, will be utilized to identify the parameters of the BMM of the $j^{\text{th}}$ sensor.

*b) Determining the parameters in Beta mixture model:* Given the dataset $\bar{D}^j_{r,i}$, parameters $\boldsymbol{\theta}^{j,r,i}_{mix}$ of the BMM can be estimated using (3). More precisely, the optimal parameters are select to fit $\bar{D}^j_{r,i}$ to maximize the following cost:

$$\underset{\boldsymbol{\theta}^{j,r,i}_{mix} \in LP^{3K}}{\text{maximize}} \ \mathcal{L}(\boldsymbol{\theta}^{j,r,i}_{mix}) \tag{4}$$

where $\mathcal{L}$ is defined in (3) for the dataset $\bar{D}^j_{r,i}$.

In this article, the MLE procedure is achieved by using the constrained optimization by linear approximation (COBYLA) algorithm which is integrated into Python's *"scipy.optimize.minimize"* package. It is noted that this package is only for minimizing rather than maximizing a function, therefore, a simple mathematical transformation will be made, and (4) will then become

$$\underset{\boldsymbol{\theta}^{j,r,i}_{mix} \in LP^{3K}}{\text{minimize}} \ -\mathcal{L}(\boldsymbol{\theta}^{j,r,i}_{mix}). \tag{5}$$

It is noted that for a fixed $N_T$, if the number of the segments is small, fewer BMMs will be used. This will reduce the complexity of the identification algorithm, at the cost of lower identification accuracy. On the other hand, each dataset $\bar{D}^j_{r,i}$ will have sufficient measurements to properly estimate the parameters of the BMM in $LP^{3K}$, leading to better estimation.

## B. Object Identification

In this section, the Bayesian-based method is adopted as the identification approach for testing the effectiveness of the proposed BMM.

Given the object to be identified, a testing measurement $\mathbf{z} = [z^1, \ldots, z^j, \ldots, z^M]^T$ can be obtained when a random grasp is performed. We can form a sequence of grasps $\mathbf{z}_{1:t} = \{\mathbf{z}_1, \ldots, \mathbf{z}_t\}$ in the iterative identification procedure.

*1) Updating the Posterior Probability the Object $o_i$:* Given the $t^{\text{th}}$ grasp in the identification stage, by applying Bayesian equation in an iterative process, the probability of object $o_i$ is computed as

$$\begin{aligned} p(o_i|\mathbf{z}_{1:t}) &= \max_{s_r, r=1,\ldots,N_s} [p(o_i, s_r|\mathbf{z}_{1:t})] \\ &= \max_{s_r, r=1,\ldots,N_s} \left[\frac{p(\mathbf{z}_t|o_i, s_r)p(o_i, s_r|\mathbf{z}_{1:t-1})}{p(\mathbf{z}_t)}\right] \end{aligned} \tag{6}$$

where $p(o_i, s_r|\mathbf{z}_{1:t})$ is the posterior probability of the object $o_i$ at segment $s_r$ given $\mathbf{z}_{1:t}$, $p(\mathbf{z}_t|o_i, s_r)$ is the likelihood of observing $\mathbf{z}_t$ given $o_i$ and $s_r$, $p(o_i, s_r|\mathbf{z}_{1:t-1})$ is the prior probability and $p(\mathbf{z}_t)$ represents the marginal likelihood.

The likelihood $p(\mathbf{z}_t|o_i, s_r)$ is calculated using the *pdf* of the BMM. Assuming each dimension of the measurement is independent, according to the conditional independence [42], $p(\mathbf{z}_t|o_i, s_r)$ can be calculated by

$$\begin{aligned} p(\mathbf{z}_t|o_i, s_r) &= p\left(z^1_t, \ldots, z^j_t, \ldots, z^M_t|o_i, s_r\right) \\ &= \prod_{j=1}^{M} p\left(z^j_t|o_i, s_r\right) = \prod_{j=1}^{M} f^{\boldsymbol{\theta}^{j,r,i}_{mix}}_{mix}(z^j_t) \end{aligned} \tag{7}$$

where $f^{\boldsymbol{\theta}^{j,r,i}_{mix}}_{mix}(z^j)$ is calculated using (2). Parameters $\boldsymbol{\theta}^{j,r,i}_{mix}$ are identified from the constructed dataset using the MLE.

The prior probability of the current iteration $t$ can be considered as the posterior probability of the last iteration $t-1$. For $t = 1$, the prior probability of each object at each segment will be considered as a uniform distribution. Therefore, the prior probability of the first iteration is set as $p(o_i, s_r|\mathbf{z}_0) = \frac{1}{\ell N_s}$.

**Algorithm 1:** Bayesian haptic object identification (presented in Section III.B).

**Input:** The constructed object dataset (in Section III.A)
The estimated parameters (in Section III.A)
**Initialize:** The iteration $t$: $t \leftarrow 0$
The stopping rule: Rule $\leftarrow \tau_g$ or $\tau_b$
The condition of stopping rule: Stop $\leftarrow false$
**while** Stop ! $= true$: **do**
  $t \leftarrow t + 1$
  Do the $t^{\text{th}}$ grasp and get the haptic measurements $\mathbf{z}_t$
  **for** each $o_i \in [o_1, o_\ell]$ **do**
    **for** each $s_r \in [s_1, s_{N_s}]$ **do**
      Calculate likelihood $p(\mathbf{z}_t|o_i, s_r)$ using (7)
      Update prior probability $p(o_i, s_r|\mathbf{z}_{1:t-1})$
    **end for**
  **end for**
  Calculate marginal likelihood $p(\mathbf{z}_t)$ using (8)
  **for** each $o_i \in [o_1, o_\ell]$ **do**
    Calculate posterior probability $p(o_i|\mathbf{z}_{1:t})$ using (6)
  **end for**
  **if** Rule $==\tau_b$ and $p(o_i|\mathbf{z}_t) \geq \tau_b$: **then**
    Stop $\leftarrow true$
  **else if** Rule $==\tau_g$ and $t \geq \tau_g$: **then**
    Stop $\leftarrow true$
  **end if**
**end while**
predicted_object_label $\leftarrow \text{argmax}_{o_i \in [o_1, o_\ell]}\, p(o_i|\mathbf{z}_{1:t})$
**Output:** predicted_object_label

The marginal likelihood $p(\mathbf{z}_t)$ is calculated as

$$p(\mathbf{z}_t) = \sum_{i=1}^{\ell} \sum_{r=1}^{N_s} p(\mathbf{z}_t|o_i, s_r) p(o_i, s_r|\mathbf{z}_{1:t-1}). \tag{8}$$

The algorithm of Bayesian haptic object identification is summarized in Algorithm 1.

## IV. Experimental Evaluation

### A. Experimental Setup

*1) Object Set:* To represent a wide range of objects with different stiffnesses, sizes, and shapes, 20 objects are selected in this article (as shown in Fig. 3). Objects $1-3$, $7-10$, and 12 are the cylindrical/spherical objects, while objects $4-6$, 11, and $13-20$ are with well-defined edges. The objects are selected with reference to the Yale-CMU-Berkeley (YCB) object and model set [43].

The descriptions of the objects will be presented in the format [explanation of the object - the material]. The material description is included to provide the physical property of the objects, while the shape is evident from Fig. 3. Objects used for this study are the following: 1) a soft drink bottle—glass; 2) a can of beetroot—metal; 3) a peppercorn dispenser—hard plastic; 4) a bottle of handwash—soft plastic; 5) a drinking mug—ceramic; 6) another drinking mug—ceramic; 7) an arbitrarily shaped 3-D-printed object—PLA plastic; 8) a second soft drink bottle—soft plastic; 9) a tennis ball—uniform felt-covered rubber compound; 10) a silicone ball—hard silicone; 11) a bottle of mouthwash—medium stiffness plastic; 12) a sports drink bottle—soft plastic; 13) a Lego block—hard plastic; 14) another drink bottle of a different shape—soft plastic; 15) a milk bottle—soft plastic; 16) a 3-D-printed apple—PLA plastic; 17) a stain remover spray bottle of nonaxisymmetric shape—medium stiffness plastic; 18) a cleaning spray bottle of nonaxisymmetric shape—medium stiffness plastic; 19) a can of meat—metal; 20) another Lego block—hard plastic.


Fig. 3. List of the object set with 20 objects.

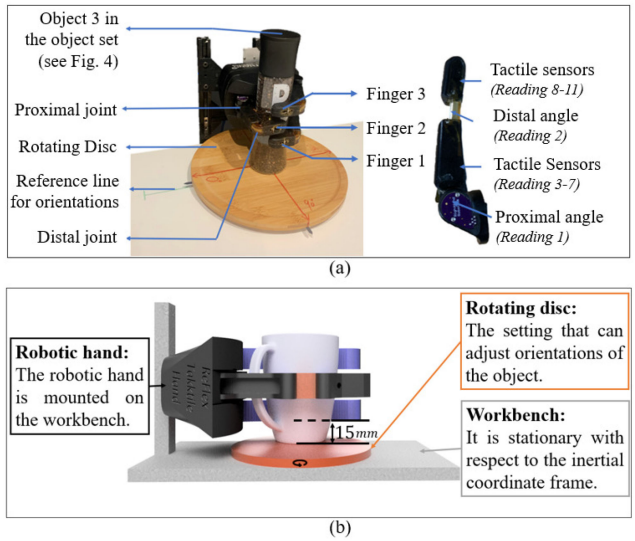


Fig. 4. Experimental platform. (a) Experimental setup. (b) Schematic of the experimental setup (side view).

*2) Robotic Hand and Sensors:* The experimental platform is shown in Fig. 4. The ReFlex TakkTile (Right Hand Robotics, US), which consists of three under-actuated fingers, is used in the study. The ReFlex hand has 4 degrees of freedom (DoFs): the flexion/extension of each finger and 1 DoF of coupled rotation between the orientation of finger $No.1$ and $No.2$). In this article,

only the 3 DoFs of finger flexion/extension are used. Each underactuated finger is controlled by an actuator that can drive the tendon spanning both the proximal and distal joints. For each finger, there is one proximal joint encoder, one tendon spool encoder, and nine Takktile pressure sensors arranged along with the finger.

The ReFlex hand is mounted on a steel frame and its three fingers are positioned parallel to the horizontal direction. When grasping an object, the object will be placed on the workbench and close to the robotic hand. The hand is positioned such that it grasps the objects 15 mm above the surface of the workbench. This height was found appropriate (sufficient) to differentiate objects in the selected object set (as shown in Fig. 4). During each grasp, all fingers are commanded to move 3 rad over 6 s to ensure that the tactile sensors mounted on the fingers properly touch the surface of the object. A torque threshold is also set for each motor. For each finger, once this threshold is reached, this finger will stop moving and keep that finger posture as the final posture for measurements.

*3) Software:* The robotic hand operation is performed via Robot Operating System (ROS), version "ROS-indigo," under Linux Ubuntu 14.04 system. The measurements (joint angle and pressure value) are recorded via "rosbag" command and is saved in the "comma-separated values"(".csv") file.

### B. Object Dataset Construction

*1) Data Acquisition and Normalization:* Each object $o_i \in O, i = 1, \ldots, 20$ in the object set is grasped in 36 different intervals about the vertical axis (from 0 to $360^o$ with the resolution of $10^o$). Hence, the number of intervals to cover the surface is $N_g = 36$. It is noted that the reason for choosing $N_g = 36$ is that collecting the haptic measurement with $10^o$ interval of the grasping pose of the robotic hand around the object allows comparing the performance of the algorithm at the different number of segments (as 36 is divisible by a good few numbers: 36, 18, 9, 6, 4 and 2). At each interval, the grasp is repeated three times ($N_T = 3$), and during each grasping, the object will be rotated to make the interval faces the robotic hand. The collected data are then normalized using the "Min–Max" normalization method.

*2) Estimation of Parameters of Beta Mixture Model:* As discussed in Section III, the parameter estimation step starts by reorganizing the measurements into segments. In the experiments, six different segment arrangements are evaluated.

1) *Case 1:* 36 segments ($n = 1$) with 3 measurements in each segment ($S = 3$).
2) *Case 2:* 18 segments ($n = 2$) with 6 measurements in each segment ($S = 6$).
3) *Case 3:* 12 segments ($n = 3$) with 9 measurements in each segment ($S = 9$).
4) *Case 4:* 6 segments ($n = 6$) with 18 measurements in each segment ($S = 18$).
5) *Case 5:* 4 segments ($n = 9$) with 27 measurements in each segment ($S = 27$).
6) *Case 6:* 2 segments ($n = 18$) with 54 measurements in each segment ($S = 54$).

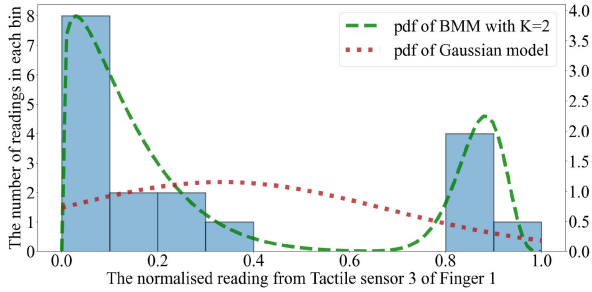


Fig. 5. Fitting result of the BMM ($K = 2$) and Gaussian model. The histogram shows the readings from tactile sensor 3 of Finger 1 in the first segment of Object 4.

In all six cases, four methods for statistical modeling are used.

1) Method 1: Gaussian model (the baseline method).
2) Method 2: BMM ($K = 1$). 2 parameters to identify.
3) Method 3: BMM ($K = 2$). 5 parameters to identify.
4) Method 4: BMM ($K = 3$). 8 parameters to identify.

### C. Object Identification

Methods 1–4 are used to identify the object. Each object will be identified six times, therefore, six trials of identification for each object are conducted for the identification methods described. The accuracy measure is obtained by taking the average of the number of times the algorithm correctly identifies the object out of the total six attempts. As the focus is to evaluate the performance of the BMM for identifying the object, in each identification trial, $\tau_g$ is set to 1, to simplify the evaluation procedure without loss of generality.

## V. Results and Discussion

### A. Object Dataset Construction

To evaluate the haptic measurements fitting performance of each sensor for each object at each segment, the "Cramer–von Mises criterion" is adopted. The "Paired t-test" is then used to statistically compare the overall performance of the BMMs and the Gaussian model for each segment. Since there are 33 sensors measuring over the different number of segments on 20 objects, as an illustrative result, only the performance of different methods at six segments (Case 4) is represented in this article. For all three BMM methods, according to the $p$-value calculated using the "Paired t-test," the BMMs demonstrated a closer fit than that of Gaussian at a significant level of 0.001. Representative distribution of tactile measurements is given in Fig. 5, which specifically shows the tactile measurements of the third tactile sensor of the first finger when grasping Object 4. Two peaks are observed, corresponding to the "no contact" and the "firm contact" cases, respectively. This is widely observed in the measurements of tactile sensors in this experiment. The resulting distribution modeled by a BMM (in this case, at $K = 2$) is shown in the figure, as well as a comparison to that with a Gaussian model.

TABLE I
ENTRIES IN BOLD INDICATE THE HIGHEST PERFORMING CASE IN EACH METHOD[1]

| | Method 1: Gaussian model | | | | | | Method 2: BMM with $K = 1$ | | | | | |
|---|---|---|---|---|---|---|---|---|---|---|---|---|
| Object | Case 1 36 segments | Case 2 18 segments | Case 3 12 segments | Case 4 6 segments | Case 5 4 segments | Case 6 2 segments | Case 1 36 segments | Case 2 18 segments | Case 3 12 segments | Case 4 6 segments | Case 5 4 segments | Case 6 2 segments |
| 4 | 66.7% | 83.3% | 66.7% | 66.7% | 100.0% | 33.3% | 100.0% | 100.0% | 100.0% | 100.0% | 100.0% | 50.0% |
| 5 | 83.3% | 100.0% | 100.0% | 100.0% | 100.0% | 100.0% | 100.0% | 100.0% | 100.0% | 100.0% | 100.0% | 100.0% |
| 6 | 66.7% | 66.7% | 50.0% | 100.0% | 100.0% | 100.0% | 83.3% | 100.0% | 100.0% | 100.0% | 83.3% | 100.0% |
| 11 | 33.3% | 66.7% | 66.7% | 66.7% | 33.3% | 16.7% | 83.3% | 50.0% | 33.3% | 33.3% | 66.7% | 16.7% |
| 13 | 66.7% | 66.7% | 83.3% | 66.7% | 66.7% | 50.0% | 100.0% | 83.3% | 83.3% | 83.3% | 83.3% | 83.3% |
| 14 | 66.7% | 83.3% | 83.3% | 83.3% | 66.7% | 100.0% | 83.3% | 100.0% | 83.3% | 83.3% | 100.0% | 100.0% |
| 15 | 33.3% | 83.3% | 50.0% | 50.0% | 50.0% | 33.3% | 66.7% | 100.0% | 100.0% | 100.0% | 100.0% | 100.0% |
| 16 | 83.3% | 83.3% | 100.0% | 100.0% | 83.3% | 83.3% | 100.0% | 83.3% | 100.0% | 100.0% | 100.0% | 100.0% |
| 17 | 33.3% | 33.3% | 33.3% | 33.3% | 33.3% | 16.7% | 66.7% | 83.3% | 83.3% | 66.7% | 50.0% | 33.3% |
| 18 | 66.7% | 66.7% | 83.3% | 83.3% | 83.3% | 33.3% | 83.3% | 100.0% | 83.3% | 50.0% | 66.7% | 16.7% |
| 19 | 83.3% | 83.3% | 83.3% | 66.7% | 50.0% | 66.7% | 83.3% | 88.3% | 50.0% | 50.0% | 50.0% | 66.7% |
| 20 | 66.7% | 66.7% | 83.3% | 50.0% | 50.0% | 33.3% | 100.0% | 100.0% | 100.0% | 100.0% | 100.0% | 83.3% |
| **Avg_nc** [2] | 62.5% | **73.6%** | **73.6%** | 72.2% | 66.7% | 55.6% | 87.5% | **90.3%** | 84.7% | 80.6% | 83.3% | 70.8% |
| **Std_nc** [2] | 0.174 | 0.153 | 0.190 | 0.200 | 0.253 | 0.335 | 0.115 | 0.138 | 0.201 | 0.225 | 0.185 | 0.307 |
| **Avg_all** [3] | 77.5% | **84.2%** | **84.2%** | 83.3% | 80.0% | 73.4% | 92.5%** | **94.2%**** | 90.8%* | 88.4% | 90.0%** | 82.5%** |
| **Std_all** [3] | 0.231 | 0.179 | 0.200 | 0.211 | 0.261 | 0.347 | 0.111 | 0.121 | 0.179 | 0.205 | 0.170 | 0.286 |

| | Method 3: BMM with $K = 2$ | | | | | | Method 4: BMM with $K = 3$ | | | | | |
|---|---|---|---|---|---|---|---|---|---|---|---|---|
| Object | Case 1 36 segments | Case 2 18 segments | Case 3 12 segments | Case 4 6 segments | Case 5 4 segments | Case 6 2 segments | Case 1 36 segments | Case 2 18 segments | Case 3 12 segments | Case 4 6 segments | Case 5 4 segments | Case 6 2 segments |
| 4 | – | 83.3% | 83.3% | 100.0% | 66.7% | 66.7% | – | – | 66.7% | 100.0% | 83.3% | 33.3% |
| 5 | – | 100.0% | 100.0% | 100.0% | 100.0% | 100.0% | – | – | 100.0% | 100.0% | 100.0% | 83.3% |
| 6 | – | 83.3% | 83.3% | 66.7% | 50.0% | 33.3% | – | – | 100.0% | 100.0% | 100.0% | 83.3% |
| 11 | – | 66.7% | 50.0% | 50.0% | 50.0% | 33.3% | – | – | 33.3% | 50.0% | 66.7% | 33.3% |
| 13 | – | 83.3% | 100.0% | 100.0% | 83.3% | 66.7% | – | – | 83.3% | 83.3% | 66.7% | 16.7% |
| 14 | – | 100.0% | 100.0% | 100.0% | 100.0% | 100.0% | – | – | 100.0% | 100.0% | 100.0% | 100.0% |
| 15 | – | 100.0% | 100.0% | 100.0% | 100.0% | 100.0% | – | – | 100.0% | 100.0% | 100.0% | 100.0% |
| 16 | – | 100.0% | 100.0% | 100.0% | 100.0% | 66.7% | – | – | 100.0% | 100.0% | 100.0% | 100.0% |
| 17 | – | 83.3% | 100.0% | 100.0% | 100.0% | 100.0% | – | – | 100.0% | 66.7% | 33.3% | 50.0% |
| 18 | – | 83.3% | 83.3% | 100.0% | 100.0% | 83.3% | – | – | 83.3% | 83.3% | 83.3% | 83.3% |
| 19 | – | 83.3% | 50.0% | 50.0% | 50.0% | 50.0% | – | – | 83.3% | 83.3% | 66.7% | 50.0% |
| 20 | – | 83.3% | 83.3% | 66.7% | 100.0% | 83.3% | – | – | 100.0% | 100.0% | 50.0% | 50.0% |
| **Avg_nc** [2] | – | **87.5%** | 86.1% | 84.7% | 83.3% | 72.2% | – | – | 87.5% | **88.9%** | 79.1% | 65.2% |
| **Std_nc** [2] | – | 0.095 | 0.171 | 0.190 | 0.207 | 0.220 | – | – | 0.186 | 0.151 | 0.208 | 0.273 |
| **Avg_all** [3] | – | **92.5%**** | 91.7%** | 90.8%** | 90.0%** | 83.3%** | – | – | 92.5%** | **93.3%**** | 87.5%* | 83.3%** |
| **Std_all** [3] | – | 0.098 | 0.154 | 0.171 | 0.186 | 0.223 | – | – | 0.162 | 0.133 | 0.196 | 0.278 |

[1]For all six cases and four methods, the identification accuracy of all cylindrical and spherical objects (Objects $1-3$, $7-10$, and 12) is 100%. Hence, only the results for noncylindrical objects (Objects $4-6$, 11, and $13-20$) are shown.
[2]Avg_nc and Std_nc denote the average and standard deviation of the identification accuracy of noncylindrical/spherical objects, respectively.
[3]Avg_all and Std_all denote the average and standard deviation of the identification accuracy of all objects, respectively.
*Note*: The values with '**' and '*' represent the identification accuracy of that method is statistically higher than that of the Gaussian model (Method 1) in the corresponding case at significance level 0.05 and 0.1 respectively.

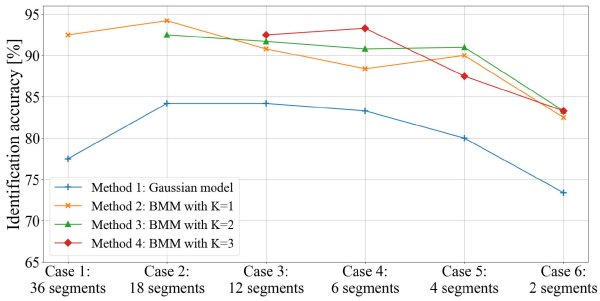


Fig. 6. Averaged identification accuracy of all objects in four methods and decreasing number of segments.

TABLE II
TWO-SAMPLE PROPORTION TEST RESULT COMPARING GAUSSIAN AND BMM ON IDENTIFICATION ACCURACY (ONE TAILED $p$-VALUE)[1]

| | Method 1 and 2 | Method 1 and 3 | Method 1 and 4 |
|---|---|---|---|
| $p$-value | $5.05 \times 10^{-7}$ | $2.34 \times 10^{-6}$ | $3.36 \times 10^{-5}$ |

[1]The $p$-value is calculated using all 20 objects in the object set and the identification result of all cases.

## B. Object Identification

The complete results of the experiment, comparing the accuracy of the haptic object identification algorithm using the Gaussian model and BMMs for all cases, are shown in Table I. The averaged accuracy is presented in Fig. 6 for ease of comparison. The $p$-values of the identification accuracy performance of the algorithm with the proposed BMMs against the Gaussian model, based on a "Two-sample proportion test," are presented in Table II to indicate the statistical significance of the difference in performance.

From Fig. 6, it can be observed that the Gaussian model (Method 1) has the lowest identification accuracy on average and BMMs (Methods 2–4) outperform the Gaussian model in all cases. The statistical significance of the difference in performance for Methods 2–4, compared to Method 1, is validated by the $p$-values presented in Table II. This supports our hypothesis that the BMM more accurately captures the distribution of the uncertainties typical in object grasping than the

Gaussian model. From Fig. 6, the identification performance can be observed to drop with the lower number of segments for all methods. This is because a lower number of segments (to represent each object) means that each Gaussian or BMM would need to capture a wider range of variations in the object, while a higher number of segments per object allows each model to capture a localized area on an object more accurately (thus, resulting in more accurate identification performance). It should be noted that a higher number of segments also means a higher number of measurements needed, as there would be a fixed number of parameters that need to be identified per segment. In our experiment, a fixed number of overall measurements was collected, thus, they are divided among the different number of segments for different cases. The cases with a higher number of segments, therefore, will have fewer measurements assigned per segment. In this case, it can be observed that for the highest number of segments and higher number of components of the BMMs (Methods 3 and 4, corresponding to $K = 2, 3$, respectively), there were insufficient measurements to produce the estimation of the parameters of the BMMs. Thus, in Fig. 6 and Table I, it can be observed that these results were not available.

According to Table I, for all four methods (the BMMs and the Gaussian model), the identification accuracy of cylindrical/spherical objects (Objects $1-3, 7-10$, and 12) was 100%. As expected, due to their cylindrical symmetric feature, the measurements were not affected by the uncertainties. The primary source of noise in these measurements is the sensor noise, which is bounded within a range that is much smaller than the variance in the distinguishing information between objects. In contrast, the better performance of the BMMs relative to the Gaussian model can be found in identifying objects with sharp, clear, or well-defined edges (Objects $4-6$, 11, and $13-20$). Due to the nature of the tactile sensors used in our experiment that individual sensors are embedded in the fingers and only measure local forces applied near its location (this is a typical nature of tactile sensors, observed in many robotic hands [44], [45]), a change in the grasping position will cause a sharp angular feature on an object to press on the adjacent tactile sensor, activating a completely different sensor in the resulting reading. Therefore, the measurements distribution of each tactile sensor will contain multiple peaks, and BMMs are able to fit such distribution better than the Gaussian model.

## VI. Conclusion

This article utilizes the BMM to characterize the uncertainties typical to haptic object identification using robotic hand grasps. The BMMs were shown to be effective in representing the distribution of the tactile measurements due to the object pose uncertainties relative to the grasping hand. The advantage of the BMM over the Gaussian model is clearly shown in the identification of objects with well-defined edges. The higher number of segments used to represent an object ($N_s$) was found to improve the precision of the model of the probability density function and this in turn results in higher accuracy in the haptic object identification.

## References


[1] W. Shaw-Cortez, D. Oetomo, C. Manzie, and P. Choong, "Robust object manipulation for tactile-based blind grasping," *Control Eng. Pract.*, vol. 92, 2019, Art. no. 104136.

[2] L. Scimeca, P. Maiolino, E. Bray, and F. Iida, "Structuring of tactile sensory information for category formation in robotics palpation," *Auton. Robots*, vol. 44, pp. 1377–1393, 2020.

[3] A. A. Shahid, J. S. V. Sesin, D. Pecioski, F. Braghin, D. Piga, and L. Roveda, "Decentralized multi-agent control of a manipulator in continuous task learning," *Appl. Sci.*, vol. 11, no. 21, 2021, Art. no. 10227.

[4] H. Van Hoof, T. Hermans, G. Neumann, and J. Peters, "Learning robot in-hand manipulation with tactile features," in *Proc. Int. Conf. Humanoid Robots*, 2015, pp. 121–127.

[5] F. Vicentini *et al.*, "PIROS: Cooperative, safe and reconfigurable robotic companion for CNC pallets load/unload stations," in *Bringing Innovative Robotic Technologies from Research Labs to Industrial End-Users*. Berlin, Germany: Springer, 2020, pp. 57–96.

[6] F. Chen, F. Cannella, C. Canali, T. Hauptman, G. Sofia, and D. Caldwell, "In-hand precise twisting and positioning by a novel dexterous robotic gripper for industrial high-speed assembly," in *Proc. IEEE Int. Conf. Robot. Autom.*, 2014, pp. 270–275.

[7] A. Aggarwal, P. Kampmann, J. Lemburg, and F. Kirchner, "Haptic object recognition in underwater and deep-sea environments," *J. Field Robot.*, vol. 32, no. 1, pp. 167–185, 2015.

[8] J. Dargahi and S. Najarian, "Human tactile perception as a standard for artificial tactile sensing–A review," *Int. J. Med. Robot. Comput. Assist. Surg.*, vol. 1, no. 1, pp. 23–35, 2004.

[9] H. Liu, Y. Wu, F. Sun, and G. Di, "Recent progress on tactile object recognition," *Int. J. Adv. Robot. Syst.*, vol. 14, no. 4, pp. 1–12, 2017.

[10] A. Faragasso, J. Bimbo, A. Stilli, H. A. Wurdemann, K. Althoefer, and H. Asama, "Real-time vision-based stiffness mapping," *Sensors*, vol. 18, no. 5, 2018, Art. no. 1347.

[11] A. J. Spiers, M. V. Liarokapis, B. Calli, and A. M. Dollar, "Single-grasp object classification and feature extraction with simple robot hands and tactile sensors," *IEEE Trans. Haptics*, vol. 9, no. 2, pp. 207–220, Apr.–Jun. 2016.

[12] M. M. Zhang, M. D. Kennedy, M. A. Hsieh, and K. Daniilidis, "A triangle histogram for object classification by tactile sensing," in *Proc. IEEE Int. Conf. Intell. Robots Syst.*, 2016, pp. 4931–4938.

[13] R. R. Ma, J. T. Belter, and A. M. Dollar, "Hybrid deposition manufacturing: Design strategies for multimaterial mechanisms via three-dimensional printing and material deposition," *J. Mech. Robot.*, vol. 7, no. 2, 2015, Art. no. 021002.

[14] S. J. Lederman and R. L. Klatzky, "Hand movements: A window into haptic object recognition," *Cogn. Psychol.*, vol. 19, no. 3, pp. 342–368, 1987.

[15] S. Funabashi *et al.*, "Object recognition through active sensing using a multi-fingered robot hand with 3D tactile sensors," in *Proc. IEEE Int. Conf. Intell. Robots Syst.*, 2018, pp. 2589–2595.

[16] S. Funabashi, G. Yan, A. Geier, A. Schmitz, T. Ogata, and S. Sugano, "Morphology-specific convolutional neural networks for tactile object recognition with a multi-fingered hand," in *Proc. IEEE Int. Conf. Robot. Autom.*, 2019, pp. 57–63.

[17] A. Schmitz, Y. Bansho, K. Noda, H. Iwata, T. Ogata, and S. Sugano, "Tactile object recognition using deep learning and dropout," in *Proc. IEEE Int. Conf. Humanoid Robots*, 2015, pp. 1044–1050.

[18] S. Luo, W. Mou, K. Althoefer, and H. Liu, "Novel tactile-SIFT descriptor for object shape recognition," *IEEE Sens. J.*, vol. 15, no. 9, pp. 5001–5009, Sep. 2015.

[19] T. Corradi, P. Hall, and P. Iravani, "Bayesian tactile object recognition: Learning and recognising objects using a new inexpensive tactile sensor," in *Proc. IEEE Int. Conf. Robot. Autom.*, 2015, pp. 3909–3914.

[20] J. A. Fishel and G. E. Loeb, "Bayesian exploration for intelligent identification of textures," *Front. Neurorobot.*, vol. 6, 2012, Art. no. 4.

[21] P. Dallaire, P. Giguére, D. Émond, and B. Chaib-Draa, "Autonomous tactile perception: A combined improved sensing and Bayesian nonparametric approach," *Robot. Auton. Syst.*, vol. 62, no. 4, pp. 422–435, 2014.

[22] J. M. Romano and K. J. Kuchenbecker, "Methods for robotic tool-mediated haptic surface recognition," in *Proc. IEEE Haptics Symp.*, 2014, pp. 49–56.

[23] N. Jamali and C. Sammut, "Majority voting: Material classification by tactile sensing using surface texture," *IEEE Trans. Robot.*, vol. 27, no. 3, pp. 508–521, Jun. 2011.

[24] S. Chitta, J. Sturm, M. Piccoli, and W. Burgard, "Tactile sensing for mobile manipulation," *IEEE Trans. Robot.*, vol. 27, no. 3, pp. 558–568, Jun. 2011.

[25] D. Xu, G. E. Loeb, and J. A. Fishel, "Tactile identification of objects using Bayesian exploration," in *Proc. IEEE Int. Conf. Robot. Autom.*, 2013, pp. 3056–3061.
[26] M. Kaboli, K. Yao, D. Feng, and G. Cheng, "Tactile-based active object discrimination and target object search in an unknown workspace," *Auton. Robots*, vol. 43, no. 1, pp. 123–152, 2019.
[27] S. J. Lederman and R. L. Klatzky, "Extracting object properties through haptic exploration," *Acta Psychol.*, vol. 84, no. 1, pp. 29–40, 1993.
[28] F. Pastor *et al.*, "Bayesian and neural inference on LSTM-based object recognition from tactile and kinesthetic information," *IEEE Robot. Autom. Lett.*, vol. 6, no. 1, pp. 231–238, Jan. 2021.
[29] L. Cao, R. Kotagiri, F. Sun, H. Li, W. Huang, and Z. M. M. Aye, "Efficient spatio-temporal tactile object recognition with randomized tiling convolutional networks in a hierarchical fusion strategy," in *Proc. AAAI Conf. Artif. Intell.*, 2016, pp. 3337–3345.
[30] H. Soh and Y. Demiris, "Incrementally learning objects by touch: Online discriminative and generative models for tactile-based recognition," *IEEE Trans. Haptics*, vol. 7, no. 4, pp. 512–525, Oct.–Dec. 2014.
[31] W. De Mulder, S. Bethard, and M.-F. Moens, "A survey on the application of recurrent neural networks to statistical language modeling," *Comput. Speech Lang.*, vol. 30, no. 1, pp. 61–98, 2015.
[32] S. Luo, J. Bimbo, R. Dahiya, and H. Liu, "Robotic tactile perception of object properties: A review," *Mechatronics*, vol. 48, pp. 54–67, 2017.
[33] A. Vellido, "The importance of interpretability and visualization in machine learning for applications in medicine and health care," *Neural Comput. Appl.*, vol. 32, no. 24, pp. 18069–18083, 2020.
[34] M. Polic, I. Krajacic, N. Lepora, and M. Orsag, "Convolutional autoencoder for feature extraction in tactile sensing," *IEEE Robot. Autom. Lett.*, vol. 4, no. 4, pp. 3671–3678, Oct. 2019.
[35] H. Liu, D. Guo, and F. Sun, "Object recognition using tactile measurements: Kernel sparse coding methods," *IEEE Trans. Instrum. Meas.*, vol. 65, no. 3, pp. 656–665, Mar. 2016.
[36] M. Madry, L. Bo, D. Kragic, and D. Fox, "ST-HMP: Unsupervised spatio-temporal feature learning for tactile data," in *Proc. IEEE Int. Conf. Robot. Autom.*, 2014, pp. 2262–2269.
[37] A. J. Dobson, *Introduction to Statistical Modelling*. Berlin, Germany: Springer, 2013.
[38] C. Walck *et al.*, *Hand-Book on Statistical Distributions for Experimentalists*. Stockholm, Sweden: Univ. Stockholm, 2007.
[39] S. R. Eliason, *Maximum Likelihood Estimation: Logic and Practice*. Thousand Oaks, CA, USA: SAGE, 1993.
[40] Y. Xia, A. Mohammadi, Y. Tan, B. Chen, P. Choong, and D. Oetomo, "On the efficiency of haptic based object identification: Determining where to grasp to get the most distinguishing information," *Front. Robot. AI*, vol. 8, 2021, Art. no. 231.
[41] A. Jain, K. Nandakumar, and A. Ross, "Score normalization in multimodal biometric systems," *Pattern Recognit.*, vol. 38, no. 12, pp. 2270–2285, 2005.
[42] A. P. Dawid, "Conditional independence in statistical theory," *J. R. Statist. Soc. Ser. B. Statist. Methodol.*, vol. 41, no. 1, pp. 1–15, 1979.
[43] B. Calli, A. Walsman, A. Singh, S. Srinivasa, P. Abbeel, and A. M. Dollar, "Benchmarking in manipulation research: Using the Yale-CMU-Berkeley object and model set," *IEEE Robot. Autom. Mag.*, vol. 22, no. 3, pp. 36–52, Sep. 2015.
[44] A. Mohammadi, Y. Tan, P. Choong, and D. Oetomo, "Flexible mechanical metamaterials enabling soft tactile sensors with multiple sensitivities at multiple force sensing ranges," *Sci. Rep.*, vol. 11, no. 1, pp. 1–9, 2021.
[45] A. Mohammadi, Y. Xu, Y. Tan, P. Choong, and D. Oetomo, "Magnetic-based soft tactile sensors with deformable continuous force transfer medium for resolving contact locations in robotic grasping and manipulation," *Sensors*, vol. 19, no. 22, 2019, Art. no. 4925.